

Single-crystal elasticity of fayalite to 12 GPa

Sergio Speziale¹ and Thomas S. Duffy

Department of Geosciences, Princeton University, Princeton, New Jersey, USA

Ross J. Angel

Department of Geosciences, Virginia Polytechnic Institute and State University, Blacksburg, Virginia, USA

Received 4 May 2004; revised 8 July 2004; accepted 24 August 2004; published 1 December 2004.

[1] Single-crystal elastic constants of a natural Fe-rich olivine ($\text{Fe}_{0.94}\text{Mn}_{0.06}\text{SiO}_4$) were determined by Brillouin scattering to 12.1 GPa. The aggregate bulk modulus, shear modulus, and their pressure derivatives are $K_{50} = 136.3$ (2) GPa, $G_0 = 51.2$ (2) GPa, $(\partial K_S/\partial P)_{T0} = 4.9$ (1), $(\partial G/\partial P)_0 = 1.8$ (1), and $(\partial^2 G/\partial P^2)_0 = -0.11$ (1) GPa^{-1} . The numbers in parentheses are 1σ uncertainties on the last digit. Our results demonstrate that both the bulk and the shear moduli of fayalite depend on the Fe/(Fe + Mg) ratio at both ambient and high pressures. The pressure derivative of the bulk modulus is very sensitive to the Fe content of olivine, while the pressure dependences of the shear modulus of Mg-rich and Fe-rich compositions are comparable. The longitudinal (C_{11} , C_{22} , C_{33}) and the off-diagonal (C_{12} , C_{13} , C_{23}) moduli of fayalite show a nearly linear dependence on pressure along the whole experimental pressure range. However, the shear constants C_{44} and C_{55} show a strongly nonlinear dependence on pressure starting at $P > 5$ GPa, more than 2 GPa above the extrapolated room temperature stability limit of fayalite. The behavior of the shear constants could be a precursor of the high-pressure amorphization of fayalite observed at 30 to 40 GPa. C_{44} is the modulus that shows the strongest tendency to soften with pressure, in disagreement with previous suggestions that C_{55} softening could trigger the structural transition of olivine to the high-pressure $\gamma\text{-Fe}_2\text{SiO}_4$. Softening of C_{44} and C_{55} is compatible with a diffusionless mechanism of the structural α - to $\gamma\text{-Fe}_2\text{SiO}_4$ transition. **INDEX TERMS:** 3909 Mineral Physics: Elasticity and anelasticity; 3924 Mineral Physics: High-pressure behavior; 3999 Mineral Physics: General or miscellaneous; 3620 Mineralogy and Petrology: Crystal chemistry; 8124 Tectonophysics: Earth's interior—composition and state (1212); **KEYWORDS:** elasticity, high-pressure, fayalite, olivine, Brillouin spectroscopy

Citation: Speziale, S., T. S. Duffy, and R. J. Angel (2004), Single-crystal elasticity of fayalite to 12 GPa, *J. Geophys. Res.*, 109, B12202, doi:10.1029/2004JB003162.

1. Introduction

[2] Fayalite is the Fe-rich end-member of the olivine solid solution series. In mineralogical models for the Earth's mantle [Ringwood, 1975; Duffy and Anderson, 1989] olivine is a major component of the upper mantle. For this reason olivine's physical properties are relevant to determine the behavior of upper mantle rocks. Because of the high magnesium content of natural olivines, the thermoelastic properties of olivines with compositions in the range between Mg_2SiO_4 and $(\text{Mg}_{0.8}\text{Fe}_{0.2})_2\text{SiO}_4$ have been the subject of extensive study. Static compression [Hazen, 1976, 1977; Kudoh and Takeuchi, 1985; Downs et al., 1996; Andraut et al., 1995; Guyot et al., 1996; Zhang, 1998], elasticity measurements by ultrasonic interferometry and ultrasound resonant spectroscopy [Webb, 1989; Isaak,

1992; Chen et al., 1996; Li et al., 1996] laser-induced phonon spectroscopy [Abramson et al., 1997] and Brillouin scattering [Zha et al., 1996, 1998] have been performed to specify the thermoelastic properties of Mg-rich olivines.

[3] We have much less knowledge of the high-pressure behavior of the Fe-rich compositions of the series. The bulk modulus of fayalite has been determined by static compression [Kudoh and Takeda, 1986; Andraut et al., 1995; Zhang, 1998]. Dynamic compression of fayalite and fayalite glass has been also performed [Chen et al., 2002]. Ultrasonic elasticity measurements have been performed on polycrystalline fayalite up to 5.2 GPa [Fukizawa and Kinoshita, 1982] while the full single-crystal elastic tensor of fayalite has been determined only to 1 GPa at 300 K, and to 700 K at 1 bar [Sumino, 1979; Webb et al., 1984; Graham et al., 1988; Wang et al., 1989; Isaak et al., 1993].

[4] A complete study of the elasticity of fayalite at high pressure can contribute to a better understanding of the effect of Fe substitution for Mg on the mechanical properties of olivines in comparison with other silicates at extreme conditions (S. Speziale et al., Compositional dependence of the elastic wave velocities of garnets, olivines and other

¹Now at Department of Earth and Planetary Science, University of California, Berkeley, California, USA.

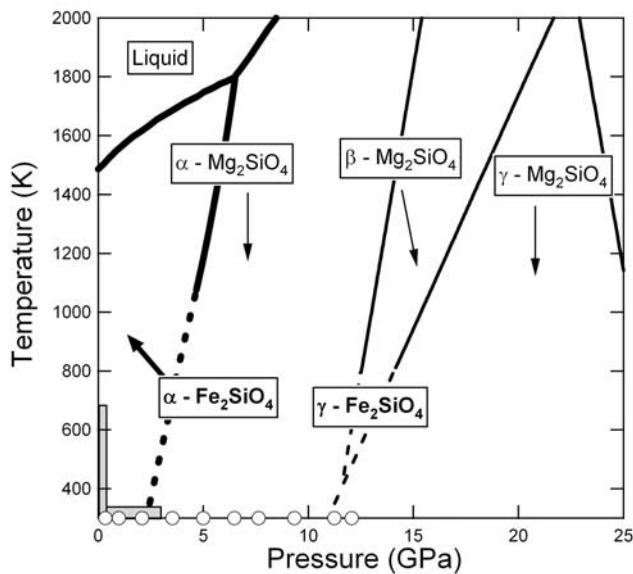


Figure 1. Phase diagram of Fe_2SiO_4 with the experimental pressure range of the present study. Shaded areas represent the explored temperature and pressure ranges in previous high-temperature and high-pressure elasticity studies of fayalite (for references, see text). The phase boundaries are from Akimoto *et al.* [1965, 1967], Yagi *et al.* [1987], and Ohtani [1979]. Heavy lines represent Fe_2SiO_4 ; light lines represent Mg_2SiO_4 . Dashed lines represent extrapolations to room temperature. Fayalite, $\alpha\text{-Fe}_2\text{SiO}_4$, was present metastably at pressures in excess of 3 GPa in this study.

mantle minerals at high pressures, submitted manuscript, 2004, hereinafter referred to as Speziale *et al.*, submitted manuscript, 2004). Fe–Mg substitution has major effects on the phase diagram of olivines. Fayalite undergoes a phase transition to a high-pressure polymorph, $\gamma\text{-Fe}_2\text{SiO}_4$ (Figure 1) with spinel structure that has been observed at pressure of 5 GPa at 1073 K [Yagi *et al.*, 1987]. The extrapolated transition pressure at room temperature is 2.75 GPa [Yagi *et al.*, 1987]; however, the high-pressure phase has not been observed by room temperature compression. The Mg-rich members of the olivine series have two different high-pressure polymorphs ($\beta\text{-Mg}_2\text{SiO}_4$, which is orthorhombic, and $\gamma\text{-Mg}_2\text{SiO}_4$, with spinel structure), and they also do not transform at ambient temperature. At pressures between 30 and 40 GPa, at room temperature fayalite loses long-range order. The X-ray diffraction peaks of fayalite broaden and weaken [Richard and Richet, 1990; Williams *et al.*, 1990; Andrault *et al.*, 1995]. Its infrared spectrum shows the appearance of new features at pressure between 20 GPa and 40 GPa [Hofmeister *et al.*, 1989] interpreted as bending modes of SiO_6 polyhedra [Williams *et al.*, 1990]. On the other hand, Raman scattering to 30 GPa does not show clear evidence of ongoing transformation [Liu and Mernagh, 1993]. The high-pressure behavior of fayalite at ambient temperature is interpreted as the effect of pressure-induced amorphization, which has been also observed in oxides and in silicates (for a review, see Sharma and Sikka [1996]). The knowledge of the pressure depen-

dence of the shear constants of fayalite can help to verify alternative hypotheses about the mechanism of the high-pressure transformation of the whole olivine solid solution series.

[5] In this study we present the results of high-pressure measurements of the elastic tensor of fayalite by Brillouin spectroscopy. It represents the first high-pressure elasticity study of a Fe-rich silicate performed with this technique. We show and interpret the effect of Fe on the mechanical behavior of olivine. The combined effect of Fe–Mg substitution in olivine and garnets is probably the most important factor to connect detectable seismic anomalies to chemical heterogeneities in the upper mantle.

2. Materials and Methods

[6] Natural single crystals of fayalite ($0.5 \times 1.0 \times 0.2$ mm size) with tabular habit flattened parallel to $\{100\}$ or $\{010\}$ from Coso Hot Spring (Inyo County, California) were cut and double-side polished to 25 or 30 μm thick platelets, both parallel and approximately orthogonal to the most developed natural faces. The platelets are optically transparent and almost colorless. The composition of the crystals, determined by electron microprobe analysis, is homogeneous and corresponds to $(\text{Fe}_{0.94}\text{Mn}_{0.06})_2\text{SiO}_4$. Even though it is not a pure end-member, hereafter we will refer to the olivine analyzed in this study as fayalite.

[7] Fayalite crystallizes in the orthorhombic system (space group Pbnm), and it is isostructural with forsterite (Mg_2SiO_4). The unit cell parameters of the sample at ambient conditions were determined by powder X-ray diffraction to be $a_0 = 4.845$ (10) \AA , $b_0 = 10.491$ (7) \AA , $c_0 = 6.063$ (9) \AA . The measured composition and unit cell volume yield a density of 4.388 (9) Mg m^{-3} . Both cell parameters and calculated density compare well with existing data of synthetic fayalite ($a_0 = 4.8195$ (6) \AA , $b_0 = 10.4788$ (17) \AA , $c_0 = 6.0873$ (8) \AA , density = 4.402 Mg m^{-3} [Fujino *et al.*, 1981]).

[8] The samples were compressed up to 12.1 GPa using a modified Merrill-Basset diamond anvil cell [Merrill and Bassett, 1974]. Brillouin scattering was measured at 10 different pressures (see Table 1 and Figure 1) along 36 directions on a platelet with orientation parallel to the natural (100) face and on a second one with orientation (0.5 1 0.2) obtained by polishing a tabular $\{010\}$ crystal. The orientation matrices of both the sample platelets were determined using the positions of 20 diffraction peaks found and centered using the Xcalibur diffractometer at Virginia Tech Crystallography laboratory. Brillouin scattering measurements were also performed for 18 directions on a randomly cut platelet with orientation (0.8 1 0.1) as determined by inversion of Brillouin data, in the pressure range between 0.3 and 5.0 GPa. The sample platelets were loaded in cylindrical chambers obtained drilling a 250- μm hole in a stainless steel gasket preindented to a thickness of 50–60 μm . A mixture of ethanol ethanol, and water (16:3:1 volume ratio) was used as a pressure medium. The Brillouin measurements were performed in symmetric forward scattering geometry with an angle of 40° between the incident and scattered beam and the normal to the diamond anvils. The average exposure time

Table 1. Best Fit Density and Isentropic Elastic Constants of Fayalite^a

Pressure, GPa	ρ , Mg m ⁻³	C ₁₁ , GPa	C ₁₂ , GPa	C ₁₃ , GPa	C ₂₂ , GPa	C ₂₃ , GPa	C ₃₃ , GPa	C ₄₄ , GPa	C ₅₅ , GPa	C ₆₆ , GPa	RMS, m s ⁻¹	Number of Data
0.3	4.3991	273 (4)	104 (4)	97 (6)	174 (2)	97 (1)	236 (1)	34.4 (3)	48 (1)	60 (1)	37	138
1.0	4.4201	274 (3)	108 (5)	100 (1)	176 (2)	99 (1)	239.3 (9)	36.0 (3)	50.3 (7)	61 (3)	53	127
2.1	4.4546	283 (4)	113 (9)	106 (1)	182 (2)	104 (1)	244.9 (3)	38.6 (3)	53 (1)	62 (2)	36	151
3.5	4.4983	289 (3)	121 (3)	114 (1)	190 (2)	109 (1)	249.2 (3)	41.8 (3)	54.0 (6)	63 (3)	36	158
5.0	4.5413	295 (3)	127 (3)	118.7 (9)	198 (2)	116 (1)	258.1 (3)	44.5 (4)	55.4 (5)	64 (3)	80	184
6.5	4.5830	305 (2)	132 (3)	126 (7)	207 (2)	121 (1)	266.9 (3)	46.0 (3)	56.7 (5)	68 (1)	46	184
7.6	4.6146	313 (2)	137 (4)	132.3 (7)	212 (2)	130 (1)	271.2 (3)	47.5 (3)	57.3 (4)	69 (1)	42	180
9.3	4.6597	318 (2)	145 (3)	137.5 (8)	221 (2)	138 (1)	277.2 (3)	48.4 (3)	58.2 (4)	71 (1)	43	186
11.3	4.7082	328 (3)	156 (3)	145 (1)	230 (2)	147 (1)	282 (1)	49.1 (4)	59.5 (5)	74 (3)	69	186
12.1	4.7289	327 (2)	160 (3)	145 (1)	234 (2)	151 (1)	283 (2)	49.0 (4)	59.5 (7)	71 (1)	71	178

^aNumbers in parentheses are 1 standard deviation uncertainty in the last digits. RMS is root-mean-square of the difference between observed and calculated sound velocities.

for each measurement was 15 min. An example spectrum collected at 5 GPa is shown in Figure 2. A total of 800 spectra were collected over the whole studied pressure range. Details about the experimental setup were reported previously by *Speziale and Duffly* [2002].

[9] Pressure determination was performed by ruby fluorescence shift [*Mao et al.*, 1986]. In all the experiments more than four ruby chips were placed as a pressure calibrant in different positions around the sample platelet. The fluorescence peaks did not show significant broadening along the whole experimental pressure range. In order to allow for possible stress relaxation after each loading step, the pressure was measured every thirty minutes after compression until complete stabilization. We observed that 4 hours were always enough for complete pressure stabilization in the sample chamber. Pressure was measured before and after every Brillouin data set collection. The time elapsed between the two sets of pressure measurements was on average 24 hours. No significant differences in pressure were detected before and after the measurements. The maximum deviation between pressure determinations at different positions in the sample chamber was always smaller than 0.2 GPa. The measurements of the different platelets were performed at the same pressure within the uncertainties in the pressure determination (± 0.1 GPa). Only for the 5.0 GPa pressure step, the pressure measured on the (100) platelet was 0.4 GPa lower than that measured in the other two platelets. In this case the velocities determined along directions in the (100) platelet were adjusted interpolating between the closest data points. The correction was in the order of 0.5% for both longitudinal and transverse acoustic velocities with an overall effect on the constants well within the estimated fitting uncertainty.

[10] To prevent the effects caused by nonparallelism of the platelet faces [*Sinogeikin and Bass*, 2000] we developed a polishing tool and a gauge system, which detects tilting to 10^{-3} degree. Vignetting effects from the body of the diamond cell [*Oliver et al.*, 1992; *Sinogeikin and Bass*, 2000] were prevented by placing diaphragms in front of the diamond cell's openings both on the incident and the scattered optical path. The accuracy and reproducibility of our system was tested by measurements of synthetic MgO and MgAl₂O₄ performed at ambient conditions in forward scattering geometry. In the range between 5.3 and 9.8 km s⁻¹, the accuracy of the velocity determination is within $\pm 0.75\%$ of the measured velocity.

The reproducibility in repeated measurements is as good as 0.5% of the measured velocity.

[11] This is the first study, to our knowledge, in which Brillouin data collected in two or three different crystal planes were simultaneously inverted to recover both the whole elastic tensor (9 constants) and the orientation of the two or three planes (6 or 9 Eulerian angles, respectively) at each pressure, for a total of 15–18 fitting parameters.

[12] The measured Brillouin scattering was converted to acoustic velocity [see *Speziale and Duffly*, 2002] by treating fayalite as optically isotropic in the data analysis. This assumption if not rigorously correct, is in fact justified by the negligible effect of the optical anisotropy of common minerals on the velocity calculation, as demonstrated in case of Brillouin measurements of carbonates, which are more anisotropic than olivines [*C.-C. Chen et al.*, 2001]. The velocities were inverted using Christoffel's equation to retrieve both elastic constants and orientation of the samples [*Every*, 1980]. The starting model for the refinement of the constants was an average of existing room pressure elasticity measurements of fayalite. The initial crystal orientation

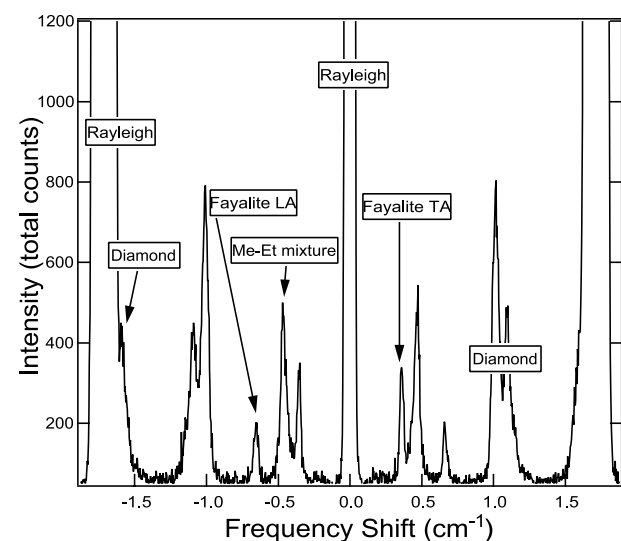


Figure 2. Brillouin spectrum of fayalite collected at 5.0 GPa. LA, quasi-longitudinal acoustic mode; TA, quasi-transverse acoustic mode; Me-Et-W, methanol-ethanol-water mixture (16:3:1 volume ratio).

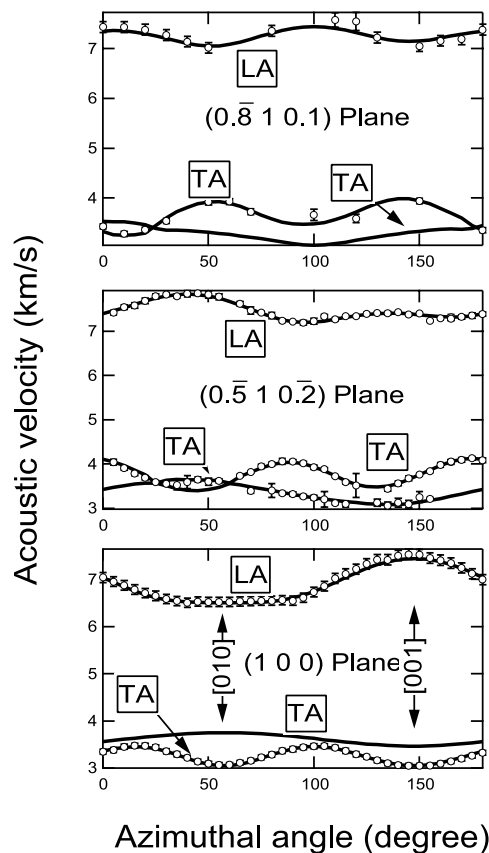


Figure 3. Velocity of the quasi-longitudinal and quasi-transverse acoustic modes in three different planes of fayalite at 3.5 GPa. The azimuthal angle is relative to an arbitrary starting direction. The curves are model velocities calculated using the best fit elastic constants. Abbreviations are as in Figure 2.

models for the (100) and the $(0.5 \ 1 \ 0.2)$ platelets were those determined by single-crystal X-ray diffraction. The orientation determined by inversion of the Christoffel's equation shows consistently 1° to 1.5° uncertainties at all the experimental pressures. The inverted orientations at all the pressures agree within 5° with the starting X-ray diffraction model. The results overlap between reciprocal uncertainties. There was not any systematic change in the inverted orientation with increasing pressure. Their variation is comparable with the estimated uncertainties. To prevent undesirable movements of the platelet in the sample chamber at pressures lower than 2 GPa, we monitored with a microscope reticle ($6 \ \mu\text{m}$ resolution) the position of the

sample in experimental conditions for as long as 12 hours, comparable with the duration of one experimental pressure step. We did not detect movements, at the resolution of our observation, in any of the samples that we analyzed.

3. Results: Effect of Composition on the Elastic Properties of Olivines

[13] At all experimental pressures we could detect two modes (quasi-longitudinal and quasi-shear) in the (100) platelet, and two or three modes (two quasi-shear and one quasi-longitudinal) in the platelet with $(0.5 \ 1 \ 0.2)$ orientation. The absence of one of the two quasi-shear modes is the result of poor elasto-optic coupling in specific crystal directions for specific polarizations of incident and scattered light [see, e.g., *Cummins and Schoen*, 1972]. After velocities and platelet orientations at all pressures were fit to Christoffel's equation, aggregate bulk and shear moduli, corresponding to the Reuss (isostress) limit, were calculated and a refined density model was determined. The procedure was iterated until it converged to a self-consistent density model after the procedure reported by *Speziale and Duffy* [2002]. The results are displayed in Table 1. Up to 5 GPa a third platelet $(0.8 \ 1 \ 0.1)$ was analyzed to check the quality of the refined elastic tensor. The results on the third platelet were always consistent with the model. An example of the overall data set collected at a single pressure is plot in Figure 3 together with the calculated velocity model from the inversion results.

[14] The robustness of the fitting results is enhanced by the large number of inverted velocities ranging between 127 and 186 at the different pressures (Table 1). The quality of the fitting is excellent as demonstrated by low root-mean-square (RMS) difference between observed and calculated velocities, which is in general equal to 1% of the overall average of the measured velocities (Table 1). The precision of the retrieved constants is always better than 2% (1σ level) for the longitudinal C_{11} , C_{22} , and C_{33} , and for the shear constants C_{44} , C_{55} and C_{66} , it is better than 5% for the off-diagonal constants C_{12} , C_{13} , and C_{23} .

[15] The Hill average [*Hill*, 1963] of the Voigt and Reuss bounds of the aggregate bulk and shear moduli were calculated at each pressure. The fit constants and the aggregate moduli retrieved at all the pressures were fit to third- or fourth-order Eulerian finite strain equations [*Davies*, 1974], to determine both zero pressure constants and their pressure derivatives, using the densities iteratively refined. The inverted zero-pressure values of the elastic constants of fayalite are given in Table 2, and their pressure derivatives in Table 3. The pressure dependence of the

Table 2. Isentropic Elastic Constants of Fayalite at Ambient Conditions^a

Study ^b	C_{11} , GPa	C_{12} , GPa	C_{13} , GPa	C_{22} , GPa	C_{23} , GPa	C_{33} , GPa	C_{44} , GPa	C_{55} , GPa	C_{66} , GPa
This study ^{c,d}	270 (2)	103 (2)	97.2 (8)	171.1 (9)	93.5 (7)	234.1 (5)	33.4 (2)	48.7 (7)	59.6 (10)
Ultrasonic interferometry A	265.85 (38)	92.4 (14)	80.6 (16)	160.30 (11)	88.4 (14)	222.42 (44)	31.55 (21)	46.74 (17)	57.15 (9)
Brillouin spectroscopy B ^d	260.3 (16)	93.9 (21)	92.5 (30)	167.6 (19)	88.5 (30)	233.6 (18)	32.9 (4)	46 (1)	55.1 (6)
Resonant ultrasound spectroscopy C	267.0 (19)	95.2 (15)	98.7 (16)	173.60 (11)	97.9 (12)	239.2 (14)	32.4 (1)	46.7 (1)	57.3 (1)
Resonant ultrasound spectroscopy D	269.0 (16)	94.4 (15)	96.9 (15)	171.6 (19)	93.7 (9)	232.5 (28)	32.4 (3)	46.5 (3)	57.4 (3)

^aNumbers in parentheses are 1 standard deviation uncertainty in the last digits.

^bStudies are A, *Graham et al.* [1988]; B, *Wang et al.* [1989], as reported by *Isaak et al.* [1993]; C, *Sumino* [1979]; D, Average of three different measurements on two specimens reported by *Isaak et al.* [1993].

^cFit results.

^d $(\text{Fe}_{0.94}, \text{Mn}_{0.06})_2\text{SiO}_4$.

Table 3. Pressure Derivatives of the Isentropic Elastic Constants of Olivines^a

Derivative	Study ^b					
	This Study (Fe _{0.94} Mn _{0.06}) ₂ SiO ₄	A Fa ₁₀₀	B Fa ₁₀₀	C Fa ₁₀	D Fa ₁₀	E Fa ₀
$\partial C_{11}/\partial P$	5.66 (25)	7.37 (55)		7.4 (1)	6.1 (2)	8.7 (9)
$\partial C_{12}/\partial P$	4.78 (30)	6.08 (19)		4.1 (1)	3.1 (1)	3.9 (2)
$\partial C_{13}/\partial P$	4.51 (11)	5.7 (10)		3.9 (1)	3.7 (2)	4.1 (4)
$\partial C_{22}/\partial P$	5.55 (14)	5.29 (38)		5.8 (1)	4.1 (3)	5.7 (2)
$\partial C_{23}/\partial P$	4.82 (10)	3.50 (40)		3.7 (1)	3.7 (1)	3.9 (2)
$\partial C_{33}/\partial P$	4.95 (7)	5.20 (38)		6.1 (1)	5.3 (3)	6.0 (4)
$\partial C_{44}/\partial P$	2.90 (11)	2.48 (18)		1.7 (2)	1.9 (2)	2.0 (1)
$\partial^2 C_{44}/\partial P^2$	-0.31 (2)			-0.01 (2)	-0.10 (2)	
$\partial C_{55}/\partial P$	1.67 (23)	1.35 (10)	1.715 (4)	1.8 (1)	2.1 (3)	1.7 (1)
$\partial^2 C_{55}/\partial P^2$	-0.15 (4)		-0.136 (3)	-0.09 (2)	-0.10 (2)	
$\partial C_{66}/\partial P$	1.63 (48)	1.70 (13)		2.0 (1)	2.7 (3)	1.9 (1)
$\partial^2 C_{66}/\partial P^2$	-0.12 (9)			-0.10 (2)	-0.10 (2)	
P max, GPa	12.1					

^aUnits for $\partial C_{ij}/\partial P$ are adimensional and for $\partial^2 C_{ij}/\partial P^2$ are GPa⁻¹. Numbers in parentheses are 1 standard deviation uncertainty in the last digits.

^bStudies are A, *Graham et al.* [1988]; B, *Webb et al.* [1984]; C, *Abramson et al.* [1997]; D, *Zha et al.* [1998]; E, *Zha et al.* [1996].

elastic constants and of the aggregate moduli is plotted in Figure 4. The zero-pressure values of the elastic constants are consistent with previous data. The values of the constants C_{55} and C_{66} are at the upper end of the extant data. C_{12} is 9% overestimated with respect to the average of three measurements by resonant ultrasound spectroscopy method [*Isaak et al.*, 1993], and it shows a somewhat large uncertainty (see Table 2). Our difficulty in constraining C_{12} , and to a lesser extent C_{66} (see uncertainties in Table 2) is related to the orientation of the examined platelets. The (100) platelet places strong constraints on C_{22} , C_{33} , C_{44} and the off-diagonal constant C_{23} , the general platelet ($0.\bar{5} 1 0.\bar{2}$) is relatively closer to (010) than to (001) so that it better constrains C_{11} , C_{33} , C_{55} and C_{13} than C_{12} and C_{66} . It has been observed in previous high-pressure Brillouin studies on low-symmetry materials that the off-diagonal constants are the ones recovered with the lowest accuracy [*Zha et al.*, 1996]. However, the spread in the literature values of the other two off-diagonal constants C_{13} and C_{23} (Table 2) is comparable or larger than the discrepancy of C_{12} determined in this study with respect to the average value from the previous studies. This is particularly striking if we consider that the measurements of *Graham et al.* [1988] and two of the three measurements averaged by *Isaak et al.* [1993] were performed on identical samples but they exhibit large differences in C_{12} , C_{13} , and C_{23} .

[16] The compositional effect (our sample has 6 mol % Mn₂SiO₄ content) cannot justify the differences between our results and ultrasonic studies of pure synthetic fayalite [*Sumino*, 1979; *Graham et al.*, 1988; *Isaak et al.*, 1993]; in fact, a Brillouin study [*Wang et al.*, 1989; *Isaak et al.*, 1993] of a natural fayalite with 5 mol % Mn₂SiO₄ content shows completely different results for C_{11} and C_{66} , which are lower than all the other extant data.

[17] In order to test the effects of correlation between the different inverted constants we calculated sound velocities at room pressure along directions on a general (hkl) plane using the different elastic models from the literature. The differences with respect to our model range between 0.4% and -1.7% in case of *Sumino* [1979], 0.1% and -2.2% for *Wang et al.* [1989], 0.4% and -1.6% for *Isaak et al.* [1993]. Larger discrepancies, ranging between 2.1% and -3.2%,

are observed in the case of *Graham et al.* [1988]. The comparison confirms that the results of our study are generally at the upper end of the overall existing data. However, the calculated velocity differences translate into absolute disagreement in the order of 25 to 200 m s⁻¹, which are comparable with the RMS of our inversions at each experimental pressure.

[18] The difference between our results and those of *Wang et al.* [1989], which are tabulated by *Isaak et al.*

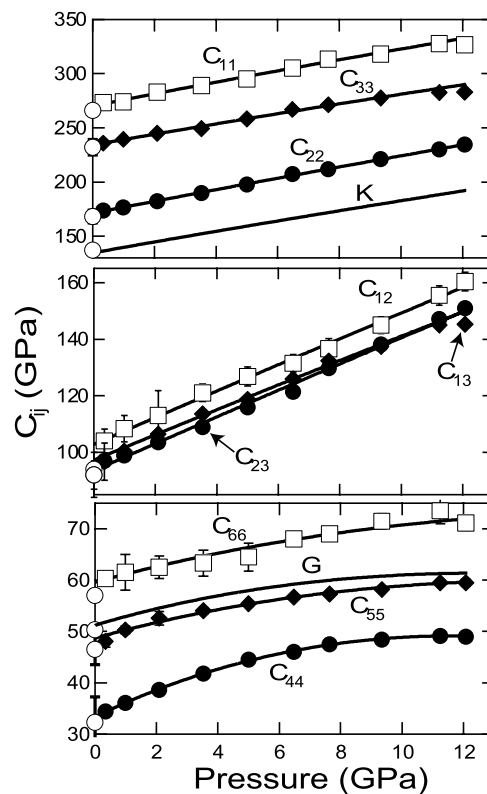


Figure 4. Individual elastic constants and Hill averages of the aggregate moduli of fayalite as a function of pressure. Lines are Eulerian strain fits to the data.

Table 4. Standard Conditions Thermodynamic and Thermoelastic Parameters of Fe₂SiO₄

Parameter	Value	Reference
Thermal expansion coefficient α	$2.61 (5) \times 10^{-5} \text{ K}^{-1}$	<i>Suzuki et al.</i> [1981]
Specific heat C_p	$67.3 \text{ J kg}^{-1} \text{ K}^{-1}$	<i>Watanabe</i> [1982]
Grüneisen parameter γ	1.19 (20)	calculated ^a
$(\partial K_T/\partial T)_{P_0}$	$-0.030 \text{ GPa K}^{-1}$	<i>Graham et al.</i> [1988]
Debye temperature θ_D	511 K	<i>Anderson and Isaak</i> [1995]

^aGrüneisen parameter obtained as $\gamma = \alpha K_S/(\rho_0 C_p)$, where ρ_0 is density at ambient conditions (Mg m^{-3}).

[1993], also obtained using Brillouin scattering on a similar natural sample could be related to the different experimental setup. Wang and coworkers performed room pressure measurements outside the diamond cell. The size of the sample could have been relatively larger than the very thin platelet used in our experiment. It is possible that the optical density of a thick fayalite crystal in the 500–550 nm wavelength range can cause a temperature increase, which can justify the low value of almost all the constants. The different magnitude of the effect on the different elastic constants is due to the intrinsic anisotropy of the optical density of fayalite [Burns, 1970]. This is much less likely to affect measurements in the diamond anvil cell because the sample is in contact with an anvil, which serves as an efficient heat sink. An order of magnitude estimation of fayalite heating at the focal spot, in the experimental setup used in our measurements gives values in the order of 30 K, which corresponds to constant softening in the order of 10^{-1} GPa, lower than the uncertainties on the inverted constants at each pressure.

[19] While there are differences between existing measurements that reflect, as discussed by *Isaak et al.* [1993], a variety of factors related to experimental errors, inversion techniques, sample heterogeneities, or defects and cleavage induced by sample preparation [see, e.g., *Webb et al.*, 1984], all the measured constants are typically consistent to within ± 2 –5% from the average of all the measurements. Only our value of C_{12} and the results of *Graham et al.* [1988] seem to be discrepant in a substantial way with the other data (Table 2).

[20] The pressure derivatives of the constants C_{11} , C_{12} , C_{13} , C_{23} from our study are significantly different from those determined by ultrasonic interferometry to 1 GPa, the only previous complete determination of the elastic tensor at high pressure [Graham et al., 1988]. This result reinforces the suspicion that some studies limited to small experimental pressure range are not always able to correctly resolve the pressure derivative of the elastic moduli [Zha et al., 1996]. On the other hand, our results for C_{55} are in excellent agreement with ultrasonic data to 3 GPa [Webb et al., 1984]. The pressure derivatives of the other constants are consistent within reciprocal uncertainties with existing ultrasonic data to 1 GPa. The shear constants C_{44} , C_{55} , and to less extent C_{66} show a nonlinear dependence on pressure (Figure 4) and, in order to determine their second-order pressure derivative, they have been fit to fourth-order Eulerian finite strain equations [Davies, 1974]:

$$C_{ijkl} = (1 + 2f)^{7/2} [C_{ijkl}^0 + a_1 f + 0.5a_2 f^2] - P\Delta_{ijkl}, \quad (1)$$

where $f = 1/2[(\rho/\rho_0)^{2/3} - 1]$ is the Eulerian finite strain, C_{ijkl}^0 is the value of the elastic constant at ambient conditions, $\Delta_{ijkl} = -\delta_{ij}\delta_{kl} - \delta_{ik}\delta_{jl} - \delta_{il}\delta_{jk}$, where δ_{xy} is the Kronecker delta, and P is the pressure. The parameter a_1 is equal to $3K_{0T}(\partial C_{ijkl}^0/\partial P + \Delta_{ijkl}) - 7C_{ijkl}^0$, where K_{0T} and $\partial C_{ijkl}^0/\partial P$ are the isothermal bulk modulus and the pressure derivative of the elastic constant C_{ijkl} at ambient conditions; a_2 is equal to $9K_{0T}^2\partial^2 C_{ijkl}^0/\partial P^2 + 3(\partial K_T/\partial P)_{T_0}(a_1 + 7C_{ijkl}^0) - 16a_1 - 49C_{ijkl}^0$, and $\partial^2 C_{ijkl}^0/\partial P^2$ and $(\partial K_T/\partial P)_{T_0}$ are the second derivative of the elastic constant and the first derivative of the isothermal bulk modulus at ambient conditions, respectively.

[21] The retrieved isentropic bulk modulus at ambient pressure and its pressure derivatives were converted to isothermal conditions by mean of thermodynamic equivalences:

$$K_{T_0} = K_{S_0}(1 + \alpha\gamma T)^{-1}, \quad (2)$$

$$(\partial K_T/\partial P)_{T_0} \cong (1 + \alpha\gamma T)^{-1} [(\partial K_S/\partial P)_{T_0} - \gamma T/K_{T_0}(\partial K_T/\partial T)_{P_0}], \quad (3)$$

where α is the thermal expansion coefficient, γ is the Grüneisen parameter, T is the temperature expressed in K, and $(\partial K_T/\partial T)_{P_0}$ is the temperature derivative of the isothermal bulk modulus at ambient conditions. The used parameters are reported in Table 4. The pressure derivative of the aggregate shear modulus is affected by the behavior of the individual shear constants. We adopted a fourth-order finite Eulerian strain equation [e.g., *Duffy and Ahrens*, 1992]:

$$G = (1 + 2f)^{5/2} (a_1 + a_2 f + 1/2a_3 f^2), \quad (4)$$

where $f = 1/2[(\rho/\rho_0)^{2/3} - 1]$ is the Eulerian strain, ρ is the density, ρ_0 is the density at ambient pressure, $a_1 = G_0$, $a_2 = 3K_{T_0}(\partial G/\partial P)_0 - 5G_0$, and $a_3 = 9\{K_{T_0}^2[(\partial^2 G/\partial P^2)_0 + 1/K_{T_0}((\partial K_T/\partial P)_{T_0} - 4)(\partial G/\partial P)_0] + 35G_0/9\}$. The Hill average of the isentropic and isothermal bulk modulus and the Hill average of the shear modulus of fayalite at ambient conditions are reported in Table 5 together with their pressure derivatives.

4. Discussion

4.1. Effect of Fe–Mg Substitution on the Elastic Properties of Olivines

[22] The aggregate bulk and shear modulus are in good agreement with existing results (Table 5) with the exception of the very low values of the bulk modulus of *Graham et al.* [1988] and of *Andrault et al.* [1995]. The results of *Andrault* and coworkers are certainly affected by high degree of nonhydrostaticity and by a large uncertainty in the pressure determination at the highest pressures in their study. On the other hand, the results of *Graham et al.* [1988] show anomalously low values of the constants C_{13} , C_{22} , C_{33} , which strongly affect the value of the bulk modulus.

[23] The pressure derivative of the bulk modulus is in agreement, within reciprocal uncertainties with that of *Graham et al.* [1988]. The pressure derivative of shear

Table 5. Hill Average of the Reuss and Voigt Aggregate Bulk and Shear Moduli of Fe₂SiO₄ and Their Pressure Derivatives at Standard Conditions^a

Study ^b	K_{50} , GPa	G_0 , GPa	$(\partial K_S/\partial P)_{T_0}$	$(\partial G/\partial P)_0$	$(\partial^2 G/\partial P^2)_0$, GPa ⁻¹	K_{T_0} , GPa	$(\partial K_T/\partial P)_{T_0}$
This study	137.57 (26)	51.22 (21)	4.85 (5)	1.79 (8)	-0.11 (1)	136.26 (21)	4.88 (5)
Ultrasonic interferometry							
A	137.9 (14)	50.9 (1)					
B	127.9 (6)	50.29 (56)	5.2 (4)	1.5 (1)			
C		52.2		1.5			
Brillouin spectroscopy D	135.8 (13)	50.9 (3)					
Resonant ultrasound spectroscopy E	134 (4)	50.7 (3)					
X-ray diffraction							
F ^c						125 (5)	4 ^d
G ^c						136 (3)	4.1 (7)
This study							
Reuss bound	134.85 (20)	49.08 (19)	5.01 (4)	2.01 (7)	-0.13 (1)	133.60 (19)	5.04 (4)
Voigt bound	140.30 (25)	55.35 (22)	4.85 (5)	1.57 (8)	-0.09 (1)	138.95 (22)	4.93 (5)

^aNumbers in parentheses are 1 standard deviation uncertainty in the last digits.

^bStudies are A, Sumino [1979]; B, Graham *et al.* [1988]; C, Fukizawa and Kinoshita [1982]; D, Wang *et al.* [1989]; E, Isaak *et al.* [1993]; F, Andrault *et al.* [1995]; G, Zhang [1998].

^cPolycrystalline sample.

^dFixed.

^eSingle crystal.

modulus is higher than existing values (Table 5). This result is justified by the larger pressure coverage of this study, which allows us to fit the curvature of the shear modulus using a fourth-order equation.

[24] The third-order Birch-Murnaghan equation of state from our Brillouin data (Figure 5) is in good agreement with static compression data below 10 GPa both for single crystal and polycrystalline samples [Kudoh and Takeda, 1986; Andrault *et al.*, 1995; Zhang, 1998]. The extrapolation of our isotherm is in disagreement with the high-pressure data of Andrault *et al.* [1995] for the same reason as discussed above. In addition, the intensity of X-ray diffraction from fayalite degrades at pressure above 10 GPa as shown by Andrault and coauthors.

[25] Because of the well-known effective stiffness of SiO₄ tetrahedra in nesosilicates [Hazen, 1976, 1977] the substitution of Fe for Mg affects the elastic properties of olivines because of the different mechanical properties of the FeO₆ octahedra with respect to the MgO₆ octahedra. The *a*-crystallographic axis in olivines is orthogonal to planes of oxygens in distorted hexagonal close packed arrangement. The *c*-crystallographic axis is parallel to chains of octahedra, which share one edge with SiO₄ tetrahedra, and the *b*-crystallographic axis is orthogonal to continuous layers of relatively soft octahedra. Crystal structure refinements at high pressure allow us to infer that the effective bulk modulus of MgO₆ in the olivine structure is in the order of 100 to 120 GPa [Hazen and Finger, 1980]. The data relative to fayalite [Kudoh and Takeda, 1986] are problematic because they are affected by nonhydrostatic conditions [Smyth *et al.*, 2000].

[26] Using the results of our Brillouin study, we calculated the isothermal linear compressibilities along the three crystallographic axes of fayalite [Nye, 1985]:

$$\partial \ln x_i / \partial P = (S_{i1} + S_{i2} + S_{i3}), \quad (5)$$

where *i* = 1, 2, 3 corresponds to the three crystallographic axes *a*, *b*, *c*, respectively. S_{ij} are the isothermal elastic compliances, in Voigt notation, defined as: $\epsilon_i = S_{ij} \sigma_j$ and calculated from the elastic constants C_{ij} .

[27] The conversion of the isentropic elastic constants to isothermal conditions was carried out in accordance to Wallace [1972]. The pressure derivatives of the individual constants were approximated according to

$$\partial C_{ij}^{0S} / \partial P - \partial C_{ij}^{0T} / \partial P = (\partial K_S / \partial P)_{T_0} - (\partial K_T / \partial P)_{T_0}. \quad (6)$$

[28] The shear constants C_{44} , C_{55} , C_{66} and their pressure derivatives do not vary between isentropic and isothermal conditions in the case of hydrostatic compression [Wallace, 1972].

[29] We compared our results with existing data of different olivine compositions by plotting axial linear compression, $(x_i - x_{i0})/x_{i0}$, versus pressure (Figure 6). The linear compressibilities along the three crystallographic axes show strong pressure dependence. The values at ambient conditions are $\partial \ln a / \partial P = 1.5 \times 10^{-3} \text{ GPa}^{-1}$, $\partial \ln b / \partial P =$

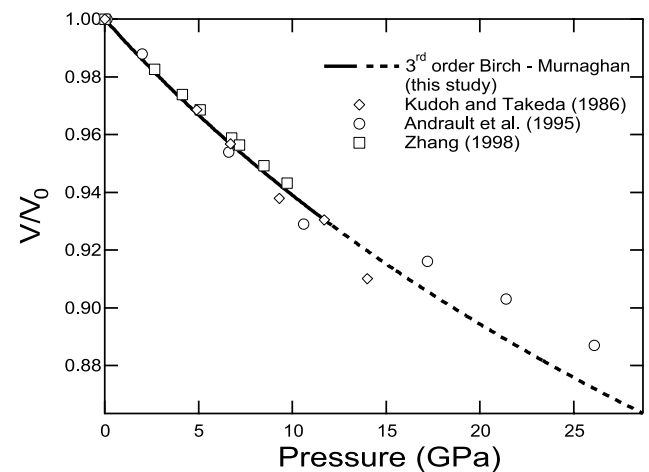


Figure 5. Third-order Birch-Murnaghan equation calculated at 300 K using the isothermal bulk modulus and its pressure derivative determined from the results of this study. Our 300 K isotherm is compared with existing static compression data.

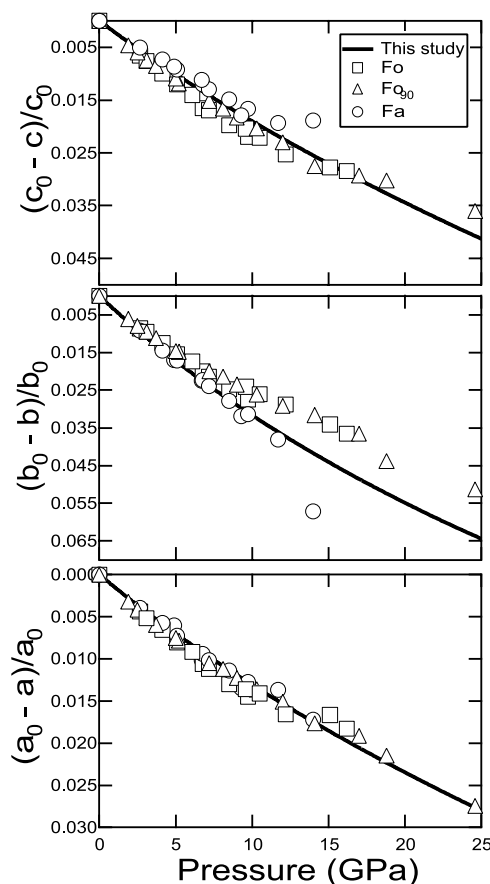


Figure 6. Axial compression of fayalite calculated from the elasticity data compared with static compression X-ray diffraction studies. Line is the calculated compression from Brillouin data. Fo, forsterite [Zha *et al.*, 1996; Zhang, 1998]; Fo₉₀, olivine with 90 mol % forsterite content [Abramson *et al.*, 1997; Zha *et al.*, 1998]; Fa, fayalite [Kudoh and Takeda, 1986; Zhang, 1998].

$3.8 \times 10^{-3} \text{ GPa}^{-1}$, and $\partial \ln c / \partial P = 2.2 \times 10^{-3} \text{ GPa}^{-1}$. They are in good agreement with the existing static compression data [Kudoh and Takeda, 1986; Zhang, 1998]. At 10 GPa our results indicate much stiffer axial compressibilities, 1.1×10^{-3} , 2.7×10^{-3} and $1.7 \times 10^{-3} \text{ GPa}^{-1}$, respectively. The calculated axial compressions along the *a* and *b* axis are in excellent agreement with those measured by Kudoh and Takeda [1986] and Zhang [1998], while the *c* axis results softer (Figure 6). The comparison with measured axial compression of Mg-rich olivines confirms that the compressibility of fayalite along the *b* axis is larger than forsterite and San Carlos olivine (Fo = 90 mol %) and both the *a* axis and *c* axis are less compressible than Mg-rich olivines (Figure 6).

[30] We also compare, in Figure 7, the pressure dependence of the aggregate moduli of fayalite with those of the Mg-rich olivines from the studies of Zha *et al.* [1996] for forsterite and Abramson *et al.* [1998] and Zha *et al.* [1998] for San Carlos olivine (Fo = 90 mol %). The Hill average of the bulk modulus of fayalite at ambient condition is equal to 137.6 (2) and is 5% higher than the value of San Carlos olivine, 7% higher than the value of forsterite. The dependence of the bulk modulus of olivine on the Fe content can

be fit to a linear relation in the pressure range examined in this study (Figure 7a). The compositional effect, $\partial K_s / \partial X$, where *X* is the molar fraction of fayalite, varies from 8.68 GPa at 1 bar to 15.8 GPa at 10 GPa. Thus the effect of Fe content on the bulk modulus is enhanced by pressure. The compositional effect is more evident when we compare the shear moduli (Figure 7b). The Hill average shear modulus of fayalite is 51.2 GPa, 37% smaller than forsterite and 35% smaller than San Carlos olivine. The dependence of the shear modulus on the molar Fe content is successfully fit to linear relations in the whole experimental pressure range. However, with increasing pressure the fit becomes less satisfactory, mainly because of the strongly nonlinear pressure dependence of the shear modulus of fayalite at pressure higher than 6 GPa (Figures 4 and 7b). With increasing pressure the compositional dependence, $\partial G / \partial X$, varies in magnitude from -30.1 GPa at ambient pressure to -34.3 GPa at 10 GPa.

[31] Our results demonstrate that the elasticity of olivines is strongly dependent on their compositions, along the whole pressure range of their stability field. In addition the pressure dependence of the chemical effect is extremely sensitive in the case of the bulk modulus. The effect of Fe content on the elasticity of olivine at high pressure has not been fully taken into account in existing mineralogical

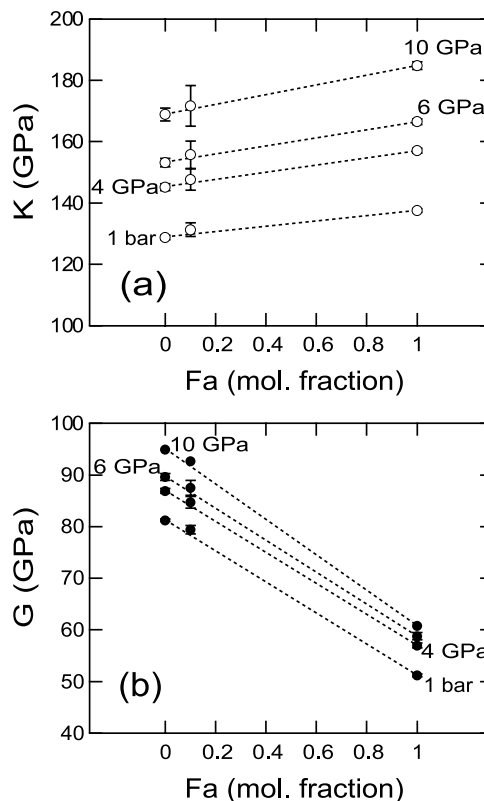


Figure 7. Variation of the isentropic aggregate moduli of olivines as a function of Fe content. (a) Bulk modulus. (b) Shear modulus. Curves are simple connections between elastic moduli of olivines with different composition. Fa = 0 mol fraction [Zha *et al.*, 1996]; Fa = 0.1 mol fraction [Abramson *et al.*, 1997; Zha *et al.*, 1998]; Fa = 1 mol fraction (this study).

Table 6. Elastic Moduli of (Mg, Fe)₂SiO₄ and Their Pressure Derivative Olivines at Ambient Conditions^a

Study	Comp., Fa mol %	Method ^b	P _{max} , GPa	K _{S0} , GPa	G ₀ , GPa	(∂K _S /∂P) _{T0}	(∂G/∂P) ₀	(∂ ² G/∂P ²) ₀ , GPa ⁻¹	K _{T0} , GPa	(∂K _T /∂P) _{T0}
This study ^c	100	BS	12.1	137.57 (26)	51.22 (21)	4.85 (5)	1.79 (8)	-0.11 (1)	136.26 (21)	4.88 (5)
A	100	UI	10 ⁻⁴	137.9 (14)	50.9 (1)					
B	100	UI	1.	127.9 (6)	50.29 (56)	5.2 (4)	1.5 (1)			
C	100	BS	10 ⁻⁴	132.2 (2)	50.5 (7)					
D	100	RUS	10 ⁻⁴	135.8 (13)	50.9 (3)					
E ^d	100	XRD	9.7						136(3)	4.1 (7)
F	11	ISAS	17	129.4	78.0	4.29	1.71	-0.054		
G	10	BS	32	131.1 (19)	78.2 (10)	3.8 (2)	1.6 (2)	-0.067 (21)		
H	10	RUS	10 ⁻⁴	129.37 (44)	78.14 (28)					
I	9	UI	3	129.4	79.1	4.65	1.95			
H	8	RUS	10 ⁻⁴	131.10 (54)	78.95 (30)					
J	0	RUS	10 ⁻⁴	128.6 (4)	81.6 (3)					
K	0	UI	6	128.7 (5)	83.8 (24)	4.2 (2)	1.7 (1)			
L ^d	0	XRD	17.2	125 (2)					125 (2)	4.0 (4)
M	0	BS	16	128.8 (5)	81.6 (2)	4.2 (2)	1.4 (1)			
E ^d	0	XRD	9.7						127 (4)	4.2 (8)

^aNumbers in parentheses are 1 standard deviation uncertainty in the last digits.

^bBS, Brillouin scattering; UI, ultrasonic interferometry; RUS, resonant ultrasound spectroscopy; XRD, X-ray diffraction; ISAS, impulsively stimulated acoustic wave spectroscopy.

^cComplete chemical composition is (Fe_{0.94}Mn_{0.06})₂SiO₄. Studies are A, *Sumino* [1979]; B, *Graham et al.* [1988]; C, *Wang et al.* [1989]; D, *Isaak et al.* [1993]; E, *Zhang* [1998]; F, *Abramson et al.* [1997]; G, *Zha et al.* [1998]; H, *Isaak* [1992]; I, *Webb* [1989]; J, *Isaak et al.* [1989]; K, *Yoneda and Morioka* [1992]; L, *Downs et al.* [1996]; M, *Zha et al.* [1996].

^dSingle crystal.

models of the upper mantle [*Duffy and Anderson*, 1989; *Ita and Stixrude*, 1993; *Vacher et al.*, 1988]. In addition, during the last years a wealth of new high-quality elasticity data have been made available, improving our knowledge of the elastic properties of many silicates and also of olivines [see *Liebermann*, 2000]. A selection of the most recent data of olivine elastic properties is given in Table 6. In order to assess how much the correct effect of composition can affect mineralogical modeling, we have computed sound velocities for olivine with Fo₉₀ (Fo 90 mol %) compositions both following a Mie-Grüneisen equation of state (as by *Ita and Stixrude* [1993]) along an isentropic pressure-temperature path with T = 1735 K at 180 km depth interpolated from *Ita and Stixrude* [1993] or applying Grüneisen theory and adiabatic finite strain equations (as

by *Duffy and Anderson* [1989] and *Vacher et al.* [1988]) along 1673 K adiabats. The properties of the intermediate compositions were computed by linear interpolation of the end-member properties, which are reported in Table 7. The shear modulus was treated with a fourth-order expansion in Eulerian strain [*Davies*, 1974]. The shear modulus of the forsterite end-member was expanded to fourth order in Eulerian strain fixing the value of (∂²G/∂P²)₀ to the value (Table 7) that causes the coefficient a₃ to vanish in equation 4. The pressure dependence of (∂²G/∂P²)₀ was neglected in our calculation. Our computations are compared with the results of the original reference models in Figure 8.

[32] The combined effects of composition and incorrect end-members properties generate sensible differences between our computations and the results of *Duffy and*

Table 7. Thermoelastic Parameters Used in the Olivine Seismic Velocity Computations^a

Parameter	Forsterite	Reference	Fayalite	Reference
ρ ₀ , Mg m ⁻³	3.222 (7)	<i>Anderson and Isaak</i> [1995]	4.388 (9)	this study
K _{T0} , GPa	127.3 (4)	<i>Isaak et al.</i> [1993]	136.26 (21)	this study
(∂K _T /∂P) _{T0}	4.2 (2) ^b	<i>Isaak et al.</i> [1989] and <i>Zha et al.</i> [1996]	4.88 (5)	this study
K _{S0} , GPa	128.7 (5)	<i>Isaak et al.</i> [1989] and <i>Zha et al.</i> [1996]	137.57 (26)	this study
(∂K _{S0} /∂P) _{T0}	4.2 (2)	<i>Isaak et al.</i> [1989] and <i>Zha et al.</i> [1996]	4.85 (5)	this study
G ₀ , GPa	81.6 (3)	<i>Isaak et al.</i> [1989] and <i>Zha et al.</i> [1996]	51.22 (21)	this study
(∂G/∂P) ₀	1.6 (2)	<i>Isaak et al.</i> [1989] and <i>Zha et al.</i> [1996]	1.15 (8)	this study
(∂ ² G/∂P ²) ₀ ^c	-0.021 (2) ^d	<i>Isaak et al.</i> [1989] and <i>Zha et al.</i> [1996]	-0.11 (8)	this study
γ ₀	1.29 (2)	<i>Anderson and Isaak</i> [1995]	1.21 (3)	<i>Anderson and Isaak</i> [1995]
θ _D , K	763	<i>Anderson and Isaak</i> [1995]	511	<i>Anderson and Isaak</i> [1995]
a ₀ , ^e K ⁻¹	3.03 × 10 ⁻⁵	<i>Suzuki</i> [1975]	2.39 × 10 ⁻⁵	<i>Suzuki et al.</i> [1981]
a ₁ , ^e K ⁻²	0.74 × 10 ⁻⁸	<i>Suzuki</i> [1975]	1.15 × 10 ⁻⁸	<i>Suzuki et al.</i> [1981]
a ₂ , ^e K	-0.538	<i>Suzuki</i> [1975]	-0.052	<i>Suzuki et al.</i> [1981]

^aNumbers in parentheses are 1 standard deviation uncertainty in the last digits. The other thermoelastic parameters were derived from *Duffy and Anderson* [1989] and *Ita and Stixrude* [1993].

^bConsidered as equal to (∂K_S/∂P)_{T0}.

^cExpressed in units of GPa⁻¹.

^dConsistent to third-order Eulerian strain fit.

^eThermal expansion coefficient expressed as α = a₀ + a₁T + a₂T⁻².

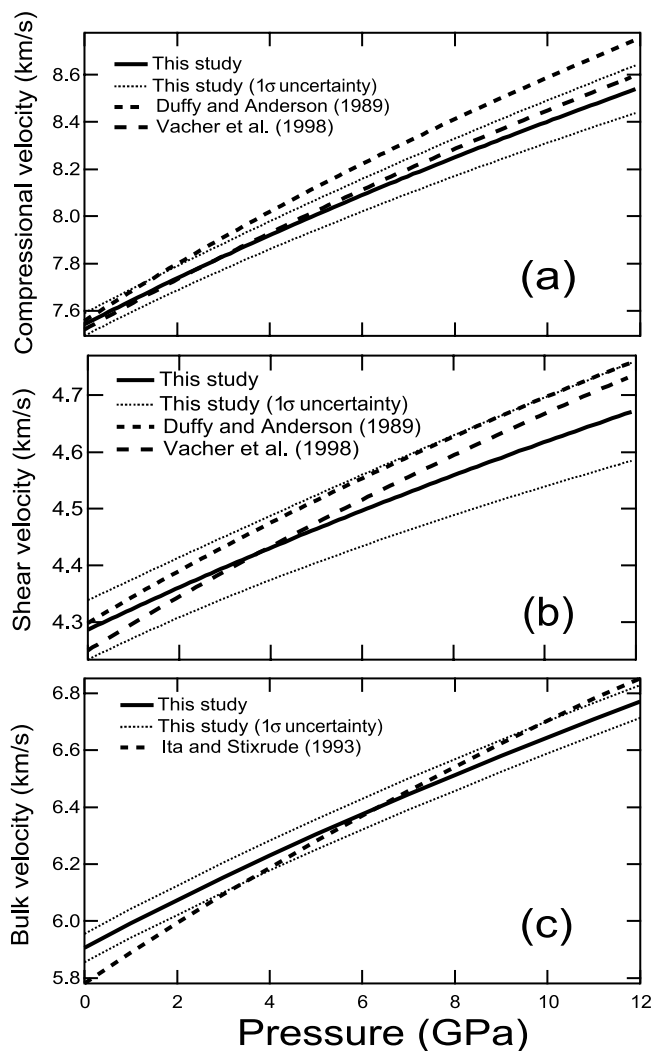


Figure 8. Comparison of model seismic velocities calculated for an olivine with Fo 90 mol % composition along isentropic pressure/temperature paths. (a) Compressional seismic velocity along the 1673 K adiabat. (b) Shear seismic velocity along the 1673 K adiabat. (c) Bulk seismic velocity of olivine Fo 90 mol %, calculated along the 1673 K isentrope for a pyrolitic composition.

Anderson [1989], which are characterized by overestimation of the pressure dependence of longitudinal velocity at pressure above 2 GPa (Figure 8a). The results of Vacher *et al.* [1988] are compatible within uncertainties with our computation.

[33] Because of the large relative uncertainty of the pressure derivative of the shear modulus, it is impossible to distinguish between our model shear velocity and the models of Duffy and Anderson [1989] and Vacher *et al.* [1988]. Nevertheless it is evident that both Duffy and Anderson and Vacher *et al.* overestimate the pressure derivative of the shear modulus (Figure 8b).

[34] The bulk sound velocity computed along a model isentropic pressure/temperature path agrees with Ita and Stixrude [1993] only below 9 GPa. The discrepancy grows to more than 1.2% at 12 GPa. The two computed velocity

models also show a clear difference in the pressure dependence of velocity (Figure 8c).

[35] The differences between our computations and the available mineralogical models increase with increasing of both pressure and Fe content because of the substantial difference in the pressure dependence of the elastic moduli of fayalite with respect to forsterite. The effect is significant in the case of the pressure dependence of the bulk modulus, which varies from 4.2 for forsterite to 4.85 for fayalite as highlighted for the first time in this study (Table 6), while it is not clear whether there is a compositional effect on the pressure dependence of the shear modulus (Table 6).

[36] These results show the need for a more correct description of the elastic properties of olivine, in order to obtain reliable upper mantle mineralogical models. In Figure 9 we plotted the combined effect of pressure and Fe enrichment or depletion on the seismic velocity of a typical peridotitic olivine (90 mol % Fo) along a 1673 K adiabat. The contours represent isobars along isentropic paths with 1673 K foot temperature. Pressures were converted to depth using the Preliminary Reference Earth Model (PREM) [Dziewonski and Anderson, 1981]. The presence of anomalously Fe-rich olivine could sensibly influence the shear seismic velocity. At 4 GPa pressure, an increase of fayalite content by 10 mol %

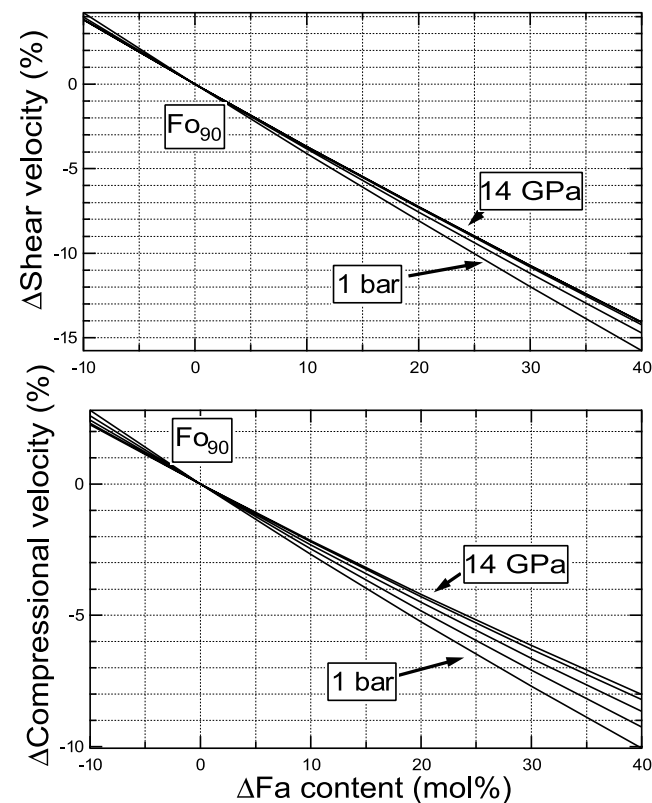


Figure 9. Relative variation of compressional and shear seismic velocity in Fe, Mg olivine as a function of Fe enrichment or depletion (expressed in mol %) with respect to Fo₉₀ “standard” peridotitic composition. The plotted isobars are 1 bar, 4 GPa, 8 GPa, 12 GPa, and 14 GPa. The isobar curves are computed as loci of points along 1673 K adiabats.

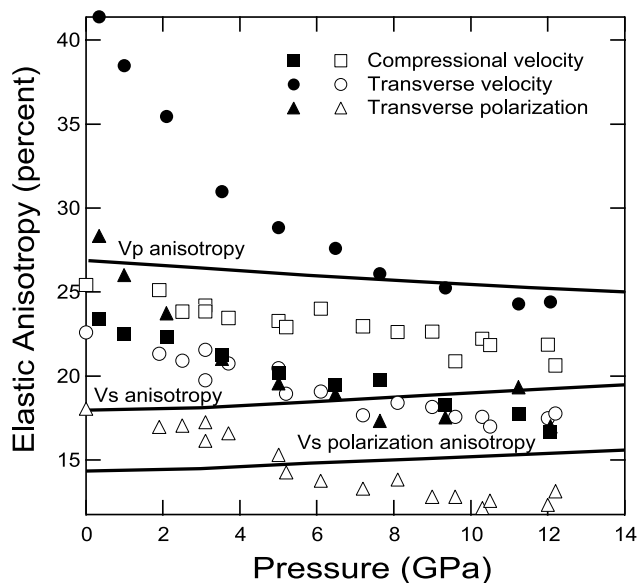


Figure 10. Elastic anisotropy of fayalite compared with Mg-rich olivine compositions. Solid symbols represent fayalite (this study). Open symbols represent San Carlos olivine, Fo_{90} [Abramson *et al.*, 1997; Zha *et al.*, 1998], and forsterite [Zha *et al.*, 1996]. Lines represent forsterite, first principles calculation [da Silva *et al.*, 1997].

would correspond to 2.4% decrease of compressional sound velocity and 3.8% decrease of shear velocity with respect to a “normal” peridotitic olivine (Fo_{90}). At 8 GPa the decrease is equal to 2.3% and 3.7%, respectively (Figure 9). The effect of fayalite content on the logarithmic variation of velocity with respect to X_{Fe} and density are discussed in a separate publication (Speziale *et al.*, submitted manuscript, 2004).

[37] To evaluate the effect of Fe enrichment on the elastic anisotropy of olivine at high pressure, we have computed at ambient temperature the values of the anisotropy in compressional, shear wave velocities and also the maximum polarization anisotropy of the shear waves in single directions [e.g., Karki *et al.*, 2001]:

$$\begin{aligned} A_P &= (V_{P_{\text{Max}}} - V_{P_{\text{Min}}})/V_P, \\ A_S &= (V_{S_{\text{Max}}} - V_{S_{\text{Min}}})/V_S, \\ A_S^{\text{PO}} &= (V_{S1} - V_{S2})_{\text{Max}}/V_S, \end{aligned} \quad (7)$$

where $V_{P_{\text{Max}}}$ is the maximum compressional velocity, $V_{P_{\text{Min}}}$ is the minimum compressional velocity, V_P is the isotropic aggregate compressional velocity, $V_{S_{\text{Max}}}$ is the maximum shear velocity in the crystal, $V_{S_{\text{Min}}}$ is the minimum shear velocity, V_S is the isotropic aggregate shear velocity, $(V_{S1} - V_{S2})_{\text{Max}}$ is the maximum value of the difference between the fast (V_{S1}) and slow (V_{S2}) shear velocities along the same direction.

[38] The net effect of Fe to Mg substitution is to increase about 100% the shear wave anisotropy (Figure 10) from 19.8% in forsterite and 21% in Fo_{90} olivine to more than 41% in fayalite at ambient conditions. Also the polarization anisotropy of the shear wave velocity is increased at ambient

pressure from 16–18% in high-Mg compositions to 28% in fayalite. The value of the compressional wave velocity anisotropy is substantially unaffected by Fe content variation with a variation from 25 to 23% from Mg-rich compositions to fayalite at room pressure (Figure 10). The pressure dependence of the compositional effect is also sensitive as can be observed in Figure 10. In fact the pressure derivative of both compressional, shear and polarization anisotropy in fayalite is higher than the corresponding of Mg-rich olivine compositions. It is interesting to observe that the results of this study show a decrease of shear elastic anisotropy with pressure, in general agreement with experimental results for forsterite and Mg-rich (Fo_{90}) olivine, but in clear disagreement with the theoretical values for forsterite [da Silva *et al.*, 1997].

[39] Because of the differences between the properties of end-member olivines it is necessary to study the behavior of intermediate compositions at high pressure in order to more fully assess the details of the compositional effect on the elastic properties of olivines at high pressure.

4.2. Metastable Behavior of Fayalite at High Pressure: Inferences From Elasticity on Amorphization and α - γ - Fe_2SiO_4 Phase Transition

4.2.1. Amorphization

[40] At ambient temperature fayalite does not undergo the equilibrium transition to its high-pressure γ -polymorph. The extrapolation of the observed limit of fayalite stability field (Figure 1) corresponds to a pressure of 2.75 GPa at ambient temperature [Yagi *et al.*, 1987]. Thus most high-pressure experimental studies on fayalite at 300 K are performed out of its thermodynamic stability field. A wide body of observations suggests that fayalite undergoes irreversible pressure-induced amorphization at pressure between 30 and 39 GPa [Richard and Richet, 1990; Williams *et al.*, 1990; Andrault *et al.*, 1995].

[41] Pressure-induced amorphization is a phenomenon which is observed in different classes of solid materials [Richet and Gillet, 1997]. Amorphization at high pressure of silicates, and especially of α - SiO_2 has attracted the interest of both the solid-state physics and the geophysical community [Hemley *et al.*, 1988; Williams and Jeanloz, 1989; Tse and Klug, 1991; Binggeli and Chelikowsky, 1992; Gregoryanz *et al.*, 2000; Haines *et al.*, 2001]. However, new results of static compression of α - SiO_2 [Haines *et al.*, 2001] suggest that some reports of high-pressure amorphization based on X-ray diffraction observations, could be biased by low X-ray power, experimental resolution, and nonhydrostatic stress conditions.

[42] The mechanism of the amorphization of fayalite is under debate, but precursors of the process can be found in a visible qualitative change in the compression mechanism observed in static compression experiments at $P > 10$ GPa [Andrault *et al.*, 1995] and in the appearance, at pressure above 30 GPa, of new infrared spectral features, which can be related to bending of SiO_6 octahedra [Williams *et al.*, 1990].

[43] The behavior of fayalite at room temperature and pressure above 30 GPa has been interpreted as (1) an effect of the metastable branch of the melting curve, which after a maximum, decreases in temperature at high pressure and intersects the compression path of metastable olivine in the

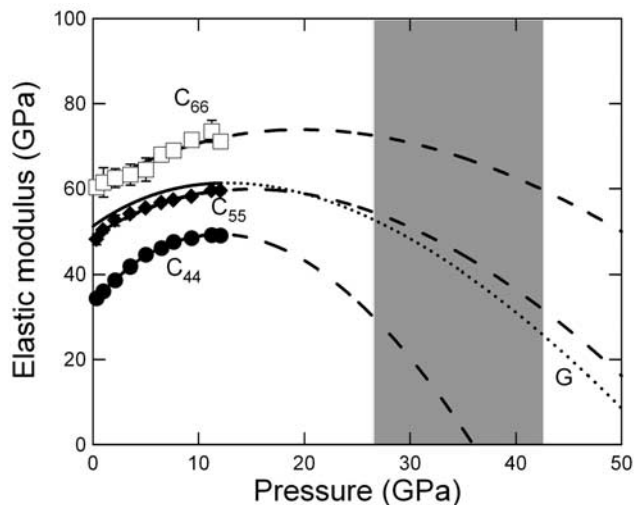


Figure 11. Extrapolated pressure dependence of the individual shear constants (C_{44} , C_{55} , C_{66}) and of the aggregate shear modulus (G) of fayalite. The extrapolation is obtained using fourth-order Eulerian strain equations. Shaded region represents the pressure range in which the phase transition takes place [Richard and Richet, 1990; Williams *et al.*, 1990; Andrault *et al.*, 1995].

stability field of γ - Fe_2SiO_4 [Richard and Richet, 1990]; and (2) as collapse of the crystalline order in metastable fayalite due to inability of the structure to satisfy geometrical and bonding constraint of the thermodynamically stable high-pressure polymorph [Williams *et al.*, 1990]. In both cases kinetic hindrance to the crystalline-crystalline phase transition leads metastable olivine to the pressure where the low-temperature amorphization occurs.

[44] The present Brillouin results show that the pressure derivative of all the three shear constants of fayalite is approaching the value of 0 at the highest limit of the experimental pressure range. Extrapolating the Eulerian finite strain equations that fit the data we can expect elastic instability at $P = 35$ GPa because of vanishing C_{44} (Figure 11). The extrapolations suggest that C_{55} and C_{66} vanish at higher pressures (57 and 76 GPa, respectively). We can estimate that in the range between 35 and 76 GPa fayalite undergoes a structural collapse or phase transition because of shear instability.

[45] It has been pointed out that shear mode softening is an indication of ongoing phase transitions, and amorphization is only one of the possible cases [Sharma and Sikka, 1996]. However, on the basis of the observation that the violation of Born's mechanical stability criteria represents only an upper bound to the onset of transformation in real solids, we can reasonably affirm that in the range between 35 and 75 GPa the softening of all the three shear constants will be so significant that it allows different pathways to instability and phase transition, and therefore it is the most probable mechanism of the only observed transition. As a consequence of the softening of all the shear constants, the extrapolated aggregate shear modulus vanishes at 56 GPa (after reaching a maximum at 12.6 GPa) thus allowing the possibility of a structural collapse with characteristics similar to thermodynamic melting.

[46] High-pressure Brillouin data suggest elastic instability of fayalite at pressure above 35 GPa, and according to accepted theoretical models of pressure-induced amorphization [Lyapin and Brazhkin, 1996] they positively confirm previous X-ray diffraction results interpreted as pressure-induced amorphization. However, the generalized softening of all the shear constants cannot unequivocally confirm or disprove either the metastable "equivalent melting" proposed by Richet and Ricard [1990] or the "frustration of linkages" proposed by Williams *et al.* [1990].

4.2.2. Phase Transition

[47] At temperatures in excess of 1073 K fayalite undergoes a phase transition at 5 GPa to γ - Fe_2SiO_4 with spinel structure [Yagi *et al.*, 1987]. The observed high-pressure high-temperature α - γ phase transition in olivines has been interpreted as (1) diffusional and (2) martensitic or pseudomartensitic. The first interpretation implies heterogeneous nucleation, especially at crystal defects and grain boundaries, and growth by diffusion of oxygen [Sung and Burns, 1976]. The second model is based on diffusionless transformation of the oxygen sublattice, from distorted hexagonal close packed (hcp) to cubic close packed (ccp), followed by synchroshear of the cations [Poirier, 1981a, 1981b] or by short-scale diffusion of cations [Furnish and Bassett, 1983; J. Chen *et al.*, 2001; Raterron *et al.*, 2002]. TEM analysis of the microstructure of the transformation products of olivines in different experimental conditions [Burnley and Green, 1989] suggests the first mechanism corresponds to equilibrium conditions, while the second is enhanced by differential stresses and nonhydrostatic conditions. However, a later TEM study of amorphous high-pressure olivine materials [Guyot and Reynard, 1992] supports the martensitic model pointing out the existence of a systematic decoupled behavior of the anion sublattice, which preserves its order, and the cation sublattice, which becomes disordered.

[48] The observed strongly nonlinear pressure dependence of the shear constants of fayalite at room temperature could be related to the mechanism of the high-pressure high-temperature α - γ phase transition. This is not in contradiction with the relevant role of elastic instability in the high-pressure low-temperature amorphization process of fayalite. The same soft mode symmetry can drive to a nonequilibrium amorphous phase at low temperature, when the phase transition to γ - Fe_2SiO_4 is hindered kinetically, and it can instead determine the equilibrium transition at the high-temperature limit through a martensitic mechanism [Lyapin and Brazhkin, 1996].

[49] Poirier [1981a, 1981b] proposed a model for the α - γ transition mechanism in forsterite on the basis of gliding along the [001] (100) slip system through combined partial dislocations and with formation of stacking faults. The elastic constant involved in the gliding is C_{55} . Softening of C_{55} would most probably activate the transition. Webb *et al.* [1984] measured the pressure dependence up to 3 GPa of C_{55} in fayalite and interpreted the absence of strong softening of the shear constant as a proof against the mechanism proposed by Poirier [1981a, 1981b].

[50] Using the temperature dependence of the shear constants of fayalite [Sumino, 1979; Isaak *et al.*, 1993] and its thermodynamic and elastic properties (see Tables 3, 4, and 7), we estimated the values of the shear constants C_{44} , C_{55}

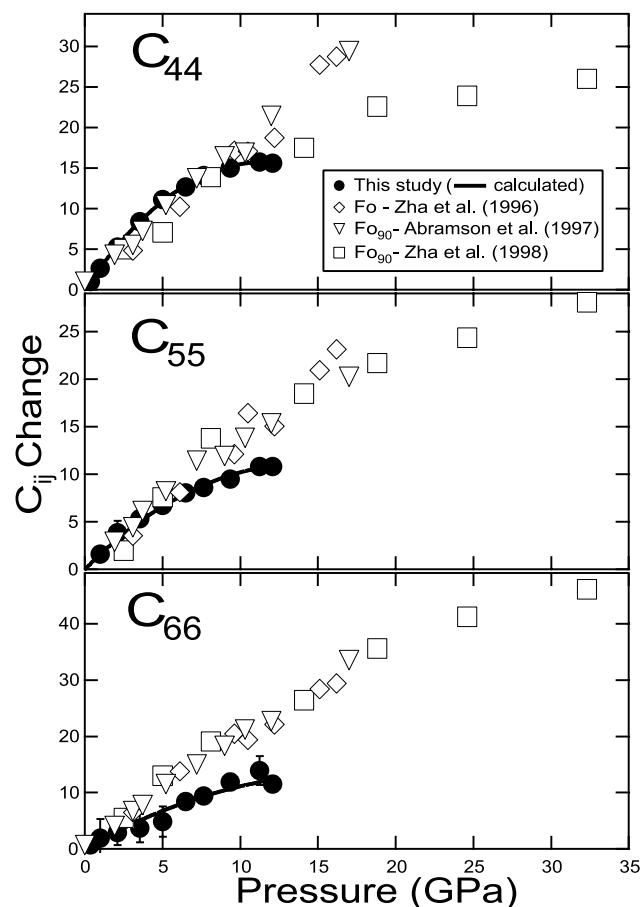


Figure 12. Change in shear elastic constants with respect to ambient pressure values for different compositions in the olivine solid solution series.

and C_{66} at 814 K and 6.5 GPa, conditions at which the phase transition was observed in quasi-hydrostatic compression in a large volume press study [Raterron *et al.*, 2002]. Neglecting, for simplicity, the cross derivative $\partial^2 C_{ij}/\partial P \partial T$ we estimated $C_{44} = 45.2$ (5) GPa, $C_{55} = 55.7$ (5) GPa, and $C_{66} = 61.0$ (5) GPa. None of the shear constants is close to instability. The ratios C_{ij}/K are equal to 0.3, 0.36 and 0.4, respectively, and they are far from the 0.15 empirical “limit value” for instability proposed by Demarest *et al.* [1977]. The cross derivative $\partial^2 C_{ij}/\partial P \partial T$ of C_{44} , C_{55} and C_{66} should be in the order of $-6.9 \times 10^{-3} \text{ K}^{-1}$, $-8.4 \times 10^{-3} \text{ K}^{-1}$, and $-9.3 \times 10^{-3} \text{ K}^{-1}$, respectively, in order to justify a shear instability at the conditions at which the transition was observed. These values are more than one order of magnitude larger than the only experimental values available of a cross derivative of a shear constant for oxides (MgO [Spetzler, 1970; Chen *et al.*, 1998]). High-temperature high-pressure elasticity data are necessary to clarify this point.

[51] It is important to stress that even taking into account the effect of temperature, the constant which shows the strongest softening is C_{44} together with C_{55} , while C_{66} softens more slowly (Figure 5). This is in disagreement with the martensitic transformation mechanism suggested by Poirier [1981a, 1981b], which would require softening of C_{55} . In addition, Raterron *et al.* [2002] report the

observation of the topotactic relation $\langle 010 \rangle \alpha\text{-Fe}_2\text{SiO}_4 / \langle 110 \rangle \gamma\text{-Fe}_2\text{SiO}_4$, in disagreement with the martensitic transformation by gliding along the $[001] (100)$ system proposed for forsterite.

[52] A comparison of the rate of change of the shear constants of fayalite with those of forsterite [Zha *et al.*, 1996] and of Fo_{90} [Abramson *et al.*, 1997; Zha *et al.*, 1998] shows that in both Fe-rich and Mg-rich olivines the constant C_{66} has the higher pressure derivative than C_{44} and C_{55} . The existing data of C_{55} in Mg-rich olivines indicate that the pressure derivative of this constant decreases with increasing Fe content. Forsterite does not show any softening of $\partial C_{55}/\partial P$ below 16 GPa (Figure 12). The existing data for C_{44} in Mg-rich olivines are somewhat less clear. Forsterite shows a linear pressure dependence of C_{44} up to 16 GPa [Zha *et al.*, 1996]. The results of the two high-pressure studies of San Carlos olivine (Fo_{90}) strongly disagree with each other. Zha *et al.* [1998] observe a strong softening of the pressure derivative of C_{44} starting before 15 GPa. At pressure above 15 GPa the rate of change of C_{44} rapidly tends to 0 (Figure 11). On the opposite the results of Abramson *et al.* [1997] are in perfect agreement with the behavior of forsterite (Figure 12).

[53] The information from high-pressure elasticity of both Mg-rich and Fe-rich olivines seems to favor the possibility of a softening of both C_{44} and C_{55} , at high pressure. C_{44} softening is not explained by the models of diffusionless transition proposed by Poirier [1981a, 1981b] and Raterron *et al.* [2002]. However, Phakey *et al.* [1972] report the presence of $[001] (010)$ slip in deformed olivines and this mechanism is geometrically consistent with softening of the constant C_{44} .

[54] We suggest that the combined effect of high-pressure/high-temperature and of substitution of Mg with Fe in the octahedral site of olivines can play a major role in favoring gliding systems which are less important at ambient conditions. Fayalite may have two active slip systems similarly convenient (energetically) to trigger the structural transition to the $\gamma\text{-Fe}_2\text{SiO}_4$ phase in different topotactic relationships between starting and final structures, as observed by Raterron *et al.* [2002].

5. Conclusions

[55] The elastic tensor of fayalite was determined to 12 GPa at 300 K. For the first time, Brillouin scattering data were simultaneously inverted for both constants and orientations of two or three different crystal planes for a total of 15–18 fit parameters. The pressure dependence of the longitudinal and off-diagonal constants is linear along the whole experimental pressure range. The shear constants C_{44} and C_{55} show strongly nonlinear pressure dependence, and their pressure derivatives are close to zero at 12 GPa. This suggests that shear softening characterizes the high-pressure behavior of metastable fayalite. We predict shear instability of fayalite in the 35 to 75 GPa pressure range in agreement with previous observation of structural collapse and amorphization and of shock-induced phase transitions.

[56] Softening of both C_{44} and C_{55} does not confirm the existing hypotheses about the mechanism of $\alpha\text{-}\gamma$ phase transition. Simultaneous softening of C_{44} and C_{55} could possibly activate two competing mechanism for a diffusion-

less transformation by gliding along the slip systems [001] (100) and [001] (010). Using a first-order linear approximation of the compositional effect with pressure, the modeled seismic velocity of the relevant upper mantle olivine (Fo_{90}) composition shows more than 1% disagreement with existing models. The pressure dependence of the elastic properties of olivines is strongly sensitive to the Fe content. An increment in Fe content from 10 mol % to 20 mol % would produce a 2.4% decrease of compressional velocity and 3.8% decrease of shear velocity at a pressure of 4 GPa along the 1673 K adiabat.

[57] **Acknowledgments.** We thank Jing Zhao for help in the orientation of the sample platelets. We thank J. Delaney (Rutgers University), who helped us to perform the microprobe chemical analysis of the samples. We also thank S. Shieh, B. Kiefer, F. Jiang, S. Hongsresawat, and the two reviewers, D. G. Isaak and I. Jackson, for their thoughtful comments and suggestions. This work was supported by the NSF and the David and Lucile Packard Foundation.

References

- Abramson, E. H., J. M. Brown, L. J. Slutsky, and J. Zaug (1997), The elastic constants of San Carlos olivine to 17 GPa, *J. Geophys. Res.*, **102**, 12,253–12,263.
- Akimoto, S., H. Fujisawa, and T. Katsura (1965), The olivine-spinel transition in Fe_2SiO_4 - Ni_2SiO_4 , *J. Geophys. Res.*, **70**, 1969–1977.
- Akimoto, S., E. Komada, and I. Kushiro (1967), Effect of pressure on the melting of olivine and spinel polymorph of Fe_2SiO_4 , *J. Geophys. Res.*, **72**, 679–686.
- Anderson, O. L., and D. G. Isaak (1995), Elastic constants of mantle minerals at high temperature, in *Mineral Physics and crystallography: A Handbook of Physical Constants*, AGU Ref. Shelf, vol. 2, edited by T. J. Ahrens, pp. 64–97, AGU, Washington, D. C.
- Andraut, D., M. A. Bouhifd, J. P. Itie, and P. Richet (1995), Compression and amorphization of $(\text{Mg,Fe})_2\text{SiO}_4$ olivines: An X-ray diffraction study up to 70 GPa, *Phys. Chem. Miner.*, **22**, 99–107.
- Binggeli, N., and J. R. Chelikowsky (1992), Elastic instability in α -quartz under pressure, *Phys. Rev. Lett.*, **69**, 2220–2223.
- Burnley, P. C., and H. W. Green II (1989), Stress dependence of the mechanism of the olivine-spinel transformation, *Nature*, **338**, 753–756.
- Burns, R. G. (1970), Crystal field spectra and evidence of cation ordering in olivine minerals, *Am. Mineral.*, **55**, 1608–1632.
- Chen, C.-C., C.-C. Lin, L.-G. Liu, S. V. Sinogeikin, and J. D. Bass (2001), Elasticity of single crystal calcite and rodocosite by Brillouin spectroscopy, *Am. Mineral.*, **86**, 1525–1529.
- Chen, G., B. Li, and R. C. Liebermann (1996), Selected elastic moduli of single crystal olivines from ultrasonic experiments to mantle pressures, *Science*, **272**, 979–980.
- Chen, G., R. C. Liebermann, and D. J. Weidner (1998), Elasticity of single-crystal MgO to 8 GPa and 1600 kelvin, *Science*, **280**, 1913–1916.
- Chen, G. Q., T. J. Ahrens, and E. M. Stolper (2002), Shock-wave equation of state of molten and solid fayalite, *Phys. Earth Planet. Inter.*, **134**, 35–52.
- Chen, J., D. J. Weidner, J. B. Parise, M. T. Vaughan, and P. Raterron (2001), Observation of cation reordering during olivine-spinel transition by in situ synchrotron X-ray diffraction at high pressure and temperature, *Phys. Rev. Lett.*, **86**, 4072–4075.
- Cummins, H. Z., and P. E. Schoen (1972), Linear scattering from thermal fluctuations, in *Laser handbook*, edited by F. T. Arecchi and E. O. Schultz-DuBois, pp. 1029–1075, North-Holland, New York.
- da Silva, C., L. Stixrude, and R. M. Wentzcovitch (1997), Elastic constants and anisotropy of forsterite at high pressure, *Geophys. Res. Lett.*, **24**, 1963–1966.
- Davies, G. F. (1974), Effective elastic moduli under hydrostatic stress, I, Quasi-harmonic theory, *J. Phys. Chem. Solids.*, **35**, 1513–1520.
- Demarest, H. M., R. Ota, and O. L. Anderson (1977), Prediction of high pressure phase transition by elastic constant data, in *High-Pressure Research: Applications in Geophysics*, edited by M. Manghnani and S. Akimoto, pp. 281–301, Academic, San Diego, Calif.
- Downs, R. T., C.-S. Zha, T. S. Duffy, and L. W. Finger (1996), The equation of state of forsterite to 17.2 GPa and effects of pressure media, *Am. Mineral.*, **81**, 51–55.
- Duffy, T. S., and T. J. Ahrens (1992), Sound velocity at high pressure and temperature and their geophysical implications, *J. Geophys. Res.*, **97**, 4503–4520.
- Duffy, T. S., and D. L. Anderson (1989), Seismic velocities in mantle minerals and the mineralogy of the upper mantle, *J. Geophys. Res.*, **94**, 1895–1912.
- Dziewonski, A. M., and D. L. Anderson (1981), Preliminary reference Earth model, *Phys. Earth Planet. Inter.*, **25**, 297–356.
- Every, A. G. (1980), General closed-form expressions for acoustic waves in elastically anisotropic solids, *Phys. Rev. B*, **22**, 1746–1760.
- Fujino, K., S. Sasaki, Y. Takeyuki, and R. Sadanaga (1981), X-ray determination of electron distribution in forsterite, fayalite and tephroite, *Acta Crystallogr.*, **B37**, 513–518.
- Fukizawa, A., and H. Kinoshita (1982), Shear velocity jump at the olivine-spinel transformation in Fe_2SiO_4 by ultrasonic measurements *in situ*, *J. Phys. Earth*, **30**, 245–253.
- Furnish, M. D., and W. A. Bassett (1983), Investigation of the mechanism of the olivine-spinel transition in fayalite by synchrotron radiation, *J. Geophys. Res.*, **88**, 10,333–10,341.
- Graham, E. K., J. A. Schwab, S. M. Sopkin, and H. Takei (1988), The pressure and temperature dependence of the elastic properties of single-crystal fayalite, *Phys. Chem. Miner.*, **16**, 186–198.
- Gregoryanz, E., R. J. Hemley, H.-K. Mao, and P. Gillet (2000), High-pressure elasticity of alpha-quartz: Instability and ferroelastic transition, *Phys. Rev. Lett.*, **84**, 3117–3120.
- Guyot, F., and B. Reynard (1992), Pressure-induced structural modifications and amorphization in olivine compounds, *Chem. Geol.*, **96**, 411–420.
- Guyot, F., Y. Wang, P. Gillet, and Y. Ricard (1996), Quasi-harmonic computations of thermodynamic parameters of olivines at high-pressure and high-temperature. A comparison with experiment data, *Phys. Earth Planet. Inter.*, **98**, 17–29.
- Haines, J., J. M. Léger, F. Gorelli, and M. Hanfland (2001), Crystalline post-quartz phase in silica at high pressure, *Phys. Rev. Lett.*, **87**, doi:10.1103/PhysRevLett.87.155503.
- Hazen, R. M. (1976), Effects of pressure and temperature on the crystal structure of forsterite, *Am. Mineral.*, **61**, 1280–1293.
- Hazen, R. M. (1977), Effects of pressure and temperature on the crystal structure of ferromagnesian olivine, *Am. Mineral.*, **62**, 286–295.
- Hazen, R. M., and L. W. Finger (1980), Crystal structure of forsterite to 40 kbar, *Carnegie Inst. Yearb.*, **79**, 364–367.
- Hemley, R. J., A. P. Jephcoat, H.-K. Mao, L. C. Ming, and M. H. Manghnani (1988), Pressure-induced amorphization of crystalline silica, *Nature*, **334**, 52–54.
- Hill, R. (1963), Elastic properties of reinforced solids: Some theoretical principles, *J. Mech. Phys. Solids*, **11**, 357–372.
- Hofmeister, A. M., J. Xu, H.-K. Mao, P. M. Bell, and T. C. Hoering (1989), Thermodynamics of Fe-Mg olivines at mantle pressures: Mid- and far-infrared spectroscopy at high-pressure, *Am. Mineral.*, **74**, 281–306.
- Isaak, D. G. (1992), High-temperature elasticity of iron-bearing olivines, *J. Geophys. Res.*, **97**, 1871–1885.
- Isaak, D. G., O. L. Anderson, T. Goto, and I. Suzuki (1989), Elasticity of single-crystal forsterite measured to 1700 K, *J. Geophys. Res.*, **94**, 5895–5906.
- Isaak, D. G., E. K. Graham, J. D. Bass, and H. Wang (1993), The elastic properties of single-crystal fayalite as determined by dynamical measurements techniques, *Pure Appl. Geophys.*, **141**, 393–414.
- Ita, J., and L. Stixrude (1993), Density and elasticity of model upper mantle compositions and their implications for whole mantle structure, in *Evolution of the Earth and Planets*, *Geophys. Monogr. Ser.*, vol. 74, edited by E. Takahashi, R. Jeanloz, and D. Rubie, pp. 111–130, AGU, Washington, D. C.
- Karki, B. B., L. Stixrude, and R. M. Wentzcovitch (2001), High-pressure elastic properties of major materials of Earth's mantle from first principles, *Rev. Geophys.*, **39**, 507–534.
- Kudoh, Y., and H. Takeda (1986), Single crystal X-ray diffraction study on the bond compressibility of fayalite, Fe_2SiO_4 and rutile, TiO_2 under high pressure, *Physica*, **139/140B**, 333–336.
- Kudoh, Y., and Y. Takeuchi (1985), The crystal structure of forsterite Mg_2SiO_4 under high pressure up to 149 kb, *Z. Kristallogr.*, **171**, 291–302.
- Li, B., G. B. Gwanmesia, and R. C. Liebermann (1996), Sound velocities of olivine and beta polymorphs of Mg_2SiO_4 at Earth's transition zone pressures, *Geophys. Res. Lett.*, **23**, 2259–2262.
- Liebermann, R. C. (2000), Elasticity of mantle minerals (experimental studies), in *Earth's Deep Interior: Mineral Physics and Tomography From the Atomic to the Global Scale*, *Geophys. Monogr. Ser.*, vol. 117, edited by S. I. Karato et al., pp. 181–199, AGU, Washington, D. C.
- Liu, L.-G., and T. P. Mernagh (1993), Raman spectra of forsterite and fayalite at high pressures and room temperature, *High Pressure Res.*, **11**, 241–256.
- Lyapin, A. G., and V. V. Brazhkin (1996), Pressure-induced lattice instability and solid-state amorphization, *Phys. Rev. B*, **54**, 12,036–12,048.

- Mao, H. K., J. Xu, and P. M. Bell (1986), Calibration of the ruby pressure gauge to 800 kbar under quasi-hydrostatic conditions, *J. Geophys. Res.*, *91*, 4673–4677.
- Merrill, L., and W. A. Bassett (1974), Miniature diamond-anvil pressure cell for single-crystal X-ray diffraction studies, *Rev. Sci. Instrum.*, *45*, 290–294.
- Nye, J. F. (1985), *Physical Properties of Crystals*, Clarendon, Oxford, U.K.
- Ohtani, E. (1979), Melting relation of Fe_2SiO_4 up to about 200 kbar, *J. Phys. Earth*, *27*, 189–208.
- Oliver, W. F., C. A. Herbst, S. M. Lindsay, and G. H. Wolf (1992), A general method for determination of Brillouin line widths by correction for instrumental effects and aperture broadening: Application to high-pressure diamond anvil cell experiments, *Rev. Sci. Instrum.*, *63*, 1884–1895.
- Phakey, P. G., Dollinger, and J. Christie (1972), Transmission electron microscopy of experimentally deformed olivine crystals, in *Flow and Fracture of Rocks*, *Geophys. Monogr. Ser.*, vol. 16, edited by H. C. Heard et al., pp. 117–138, AGU, Washington, D. C.
- Poirier, J. P. (1981a), Martensitic olivine-spinel transformation and plasticity of the mantle transition zone, in *Anelasticity in the Earth*, *Geodyn. Ser.*, vol. 4, edited by M. S. Paterson and A. Nicolas, pp. 113–117, AGU, Washington, D. C.
- Poirier, J. P. (1981b), On the kinetics of olivine-spinel transition, *Phys. Earth Planet. Inter.*, *26*, 179–187.
- Raterron, P., J. Chen, and D. J. Weidner (2002), A process for low-temperature olivine-spinel transition under quasi-hydrostatic stress, *Geophys. Res. Lett.*, *29*(10), 1401, doi:10.1029/2002GL015003.
- Richard, G., and P. Richet (1990), Room temperature amorphization of fayalite and high pressure properties of Fe_2SiO_4 liquid, *Geophys. Res. Lett.*, *17*, 2093–2096.
- Richet, P., and P. Gillet (1997), Pressure-induced amorphization of minerals: A review, *Eur. J. Mineral.*, *9*, 907–933.
- Ringwood, A. E. (1975), *Composition and Petrology of the Earth's Mantle*, McGraw-Hill, New York.
- Sharma, S. M., and S. K. Sikka (1996), Pressure induced amorphization of materials, *Prog. Mater. Sci.*, *40*, 1–77.
- Sinogeikin, S. V., and J. D. Bass (2000), Single-crystal elasticity of pyrope and MgO to 20 GPa by Brillouin scattering in the diamond anvil cell, *Phys. Earth Planet. Inter.*, *120*, 43–62.
- Smyth, J. R., S. D. Jacobsen, and R. M. Hazen (2000), Comparative crystal chemistry of orthosilicates, in *High-Temperature and High-Pressure Crystal Chemistry*, *Rev. Mineral. Geochem.*, vol. 41, edited by R. M. Hazen and R. T. Downs, pp. 187–209, Mineral. Soc. of Am., Washington, D. C.
- Spetzler, H. (1970), Equation of state of polycrystalline and single crystal MgO to 8 kbar and 800 K, *J. Geophys. Res.*, *75*, 2073–2078.
- Speziale, S., and T. S. Duffy (2002), Single-crystal elastic constants of fluorite (CaF_2) to 9.3 GPa, *Phys. Chem. Miner.*, *29*, 465–472.
- Sumino, Y. (1979), The elastic constants of Mn_2SiO_4 , Fe_2SiO_4 , and Co_2SiO_4 , and the elastic properties of olivine group minerals at high temperature, *J. Phys. Earth.*, *27*, 209–238.
- Sung, C. M., and R. G. Burns (1976), Kinetics of the olivine-spinel transition: Implications to deep focus earthquake genesis, *Earth Planet. Sci. Lett.*, *32*, 165–170.
- Suzuki, I. (1975), Thermal expansion of periclase and olivine, and their anharmonic properties, *J. Phys. Earth.*, *23*, 145–159.
- Suzuki, I., K. Seya, H. Takai, and Y. Sumino (1981), Thermal expansion of fayalite, *Phys. Chem. Miner.*, *1*, 60–63.
- Tse, J. S., and D. D. Klug (1991), Mechanical instability of α -quartz: A molecular dynamic study, *Phys. Rev. Lett.*, *67*, 3559–3562.
- Vacher, P., A. Moquet, and C. Sotin (1988), Computation of seismic profiles from mineral physics: The importance of the non-olivine components for explaining the 660 depth discontinuity, *Phys. Earth Planet. Inter.*, *196*, 275–298.
- Wallace, D. C. (1972), *Thermodynamics of Crystals*, John Wiley, Hoboken, N. J.
- Wang, H., J. D. Bass, and G. R. Rossman (1989), Elastic properties of Fe-bearing pyroxenes and olivines (abstract), *Eos Trans. AGU*, *70*, 474.
- Watanabe, H. (1982), Thermodynamical properties of synthetic high-pressure compounds relevant to earth's mantle, in *High Pressure Research in Geophysics*, *Adv. Earth Planet. Sci.*, vol. 12, edited by S. Akimoto and M. H. Manghnani, pp. 441–464, Cent. for Acad. Publ., Tokyo.
- Webb, S. L. (1989), The elasticity of the upper mantle orthosilicates olivine and garnet to 3 GPa, *Phys. Chem. Miner.*, *16*, 684–692.
- Webb, S. L., I. Jackson, and H. Takei (1984), On the absence of shear mode softening in single-crystal fayalite at high pressure and room temperature, *Phys. Chem. Miner.*, *11*, 167–171.
- Williams, Q., and R. Jeanloz (1989), Static amorphization of anorthite at 300 K and comparison with diaplectic glass, *Nature*, *338*, 413–415.
- Williams, Q., E. Knittle, R. Reichlin, S. Martin, and R. Jeanloz (1990), Structural and electronic properties of Fe_2SiO_4 -fayalite at ultrahigh pressure: Amorphization and gap closure, *J. Geophys. Res.*, *95*, 21,549–21,563.
- Yagi, T., M. Akaogi, O. Shimomura, T. Suzuki, and S. Akimoto (1987), In situ observation of the olivine-spinel phase transformation in Fe_2SiO_4 using synchrotron radiation, *J. Geophys. Res.*, *92*, 6207–6213.
- Yoneda, A., and M. Morioka (1992), Pressure derivatives of elastic constants of single crystal forsterite, in *High-Pressure Research: Application to Earth and Planetary Sciences*, edited by Y. Syono and M. H. Manghnani, pp. 207–214, AGU, Washington, D. C.
- Zha, C.-S., T. S. Duffy, R. T. Downs, H.-K. Mao, and R. J. Hemley (1996), Sound velocity and elasticity of single-crystal forsterite to 16 GPa, *J. Geophys. Res.*, *101*, 17,535–17,545.
- Zha, C.-S., T. S. Duffy, R. T. Downs, H.-K. Mao, and R. J. Hemley (1998), Brillouin scattering and X-ray diffraction of San Carlos olivine: Direct pressure determination to 32 GPa, *Earth Planet. Sci. Lett.*, *159*, 25–33.
- Zhang, L. (1998), Single crystal hydrostatic compression of (Mg, Mn, Fe, Co) $_2\text{SiO}_4$ olivines, *Phys. Chem. Miner.*, *25*, 308–312.

R. J. Angel, Department of Geosciences, Virginia Tech, Blacksburg, VA 24061, USA.

T. S. Duffy, Department of Geosciences, Princeton University, Princeton, NJ 08544, USA.

S. Speziale, Department of Earth and Planetary Science, University of California, Berkeley, CA 94720, USA. (speziale@uclink.berkeley.edu)